PAPER

Check for updates

Stress-induced tip engineering of micro-hyperbolic structures for enhanced liquid repellency

Chorong Kim,†[a] Yoonjin Lee,†[a] Jaekyoung Kim,†[a] Ji Hoon Kim [ID] *[b] and Hyunsik Yoon [ID] *[ab]

Surface functionality in micro- and nanostructured materials is highly sensitive to geometric modifications, yet methods that enable fine structural tuning through facile and scalable fabrication remain limited. We report a method to induce controlled tip bending in micro-hyperbolic (MH) structures *via* metal-specific thin film deposition. When a metal layer is thermally evaporated onto the polymeric MH structures, residual stress drives directional tip deformation: tensile stress from gold (Au) causes bending toward the metal-coated side, while compressive stress from aluminum (Al) induces bending toward the polymer side. The bending magnitude is governed by the initial taper angle and explained by Stoney's formula. The resulting tip-modified MH (TMH) structures and their polymer replicas exhibit doubly re-entrant geometries that enable robust and durable liquid repellency, even against low-surface-tension liquids such as hexadecane. This approach simplifies microscale geometric tuning and supports scalable replication, offering practical utility in liquid manipulation, adhesion control, and engineered surface functionality.

Introduction

Bioinspired micro- and nanostructures have been extensively studied for decades across various fields, including wetting,[1–5] adhesion,[6–10] optics,[11–14] and energy harvesting.[15–17] A notable feature of these structures is that even subtle changes in geometry can drastically alter surface properties.[18] A representative example is the re-entrant structure, exemplified by the nanostructured cuticle of springtails,[19,20] which can be realized by introducing a slight overhang at the tip of a micropillar. This inward-curved geometry directs the interfacial tension upward, generating a positive Laplace pressure that stabilizes trapped air beneath the liquid. As a result, the liquid remains suspended on top of the texture, maintaining the Cassie state and exhibiting greatly enhanced liquid repellency.[5] However, a simple overhang geometry is ineffective for low-surface-tension liquids, where the surface tension falls below the threshold required to maintain the meniscus curvature determined by the structural geometry. As a result, the liquid penetrates into the cavities and displaces the trapped air. To overcome this limitation, doubly re-entrant structures have been proposed,[21] characterized by two successive bends that cause the tip to face downward and introduce additional curvature. This geometry stabilizes air pockets by sustaining positive Laplace pressure even against low-surface-tension liquids, enabling nearly complete repellency across

a broad range of liquids.[21–24] Nevertheless, precise control of micro- and submicrometer-scale features typically relies on complex and costly fabrication techniques, such as two-photon lithography and reactive ion etching, which hinder large-scale implementation.[25–27] In addition, most reported omniphobic surfaces rely on fluorinated coatings to lower surface energy, which further complicates fabrication and raises growing environmental concerns associated with persistent fluorinated compounds.[28,29]

Here, we introduce a simple and scalable strategy to overcome these limitations by refining re-entrant geometries through stress-induced tip bending during metal deposition. When a metal layer is deposited *via* thermal evaporation onto micro-hyperbolic (MH) structures formed by capillary wrapping, interfacial residual stress bends the polymer tips in a controlled manner. The direction and extent of this deformation can be tuned by selecting the metal type and adjusting the initial geometry. The resulting tip-modified micro-hyperbolic (TMH) structures can be replicated in various polymeric materials through double replica molding. Compared with the original MH structures, TMH replicas exhibit enhanced liquid repellency under both static and dynamic conditions, providing a fluorine-free and scalable route to geometrically engineered surfaces for applications in microfabrication, adhesion tuning, and controlled liquid interaction.

Results and discussion

Strategy for tip engineering of MH structures through metal-specific deposition

Fig. 1 illustrates the fabrication of MH structures *via* capillary wrapping and their transformation into TMH structures

[a]Department of Chemical and Biomolecular Engineering, Seoul National University of Science and Technology, Seoul, 01811, Republic of Korea. E-mail: hsyoon@seoultech.ac.kr
[b]Energy and Environment Research Institute, Seoul National University of Science and Technology, Seoul, 01811, Republic of Korea. E-mail: jubro@seoultech.ac.kr
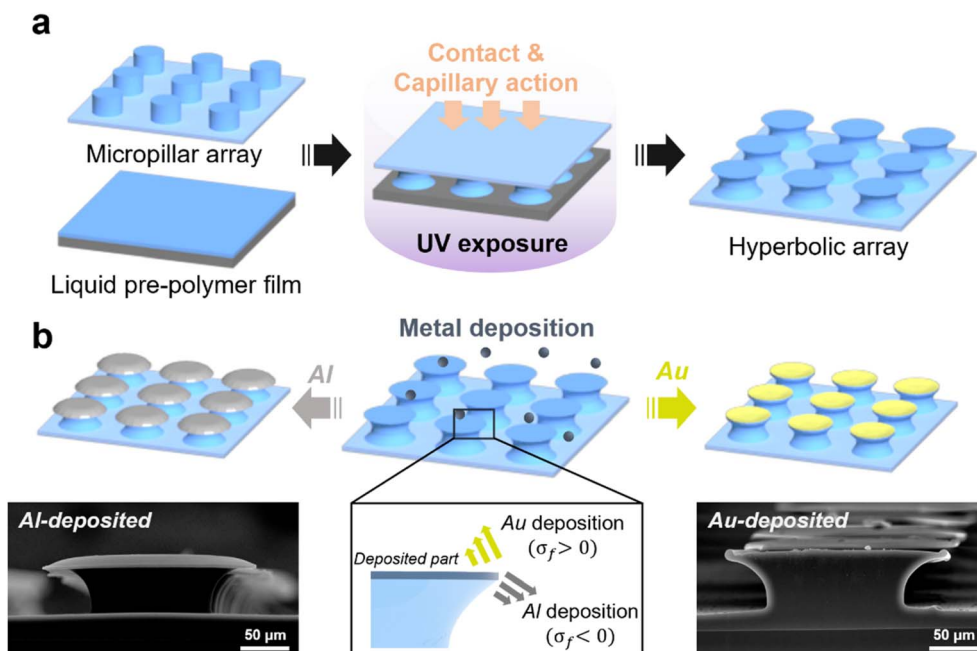† Equal contributions.

Fig. 1 Tip engineering strategy for MH structures *via* metal–specific deposition: (a) schematic of MH array formation by capillary wrapping of a photocurable prepolymer around micropillars. (b) Schematic and SEM images showing tip bending induced by residual stress from different metal types.

through metal thin-film deposition. A polyurethane acrylate (PUA) micropillar array is first fabricated, along with a thin PUA prepolymer film prepared by spin coating. When the array is gently brought into contact with the film, the liquid climbs along the pillar sidewalls and wraps around them due to capillary action, forming hyperbolic shapes (Fig. 1a). After allowing sufficient stabilization time for the viscous prepolymer during which viscous forces become negligible, UV light is applied to solidify the MH structures. The underlying mechanism and fabrication details of capillary wrapping are described in previous studies.[30,31] Subsequently, a thin metal film (thickness ∼40 nm) is deposited onto the MH structures using thermal evaporation, inducing directional bending of the MH tips, as shown in Fig. 1b. This deformation arises from residual stress in the metal film, which varies depending on the metal type. Most metals such as gold (Au) and chromium (Cr) contract

upon cooling after vapor-phase deposition due to thermal shrinkage, resulting in tensile residual stress ($\sigma_\mathrm{f} > 0$), where σ_f denotes the residual stress in the film.[32] As the underlying substrate restricts this contraction, the stress causes the tips to bend toward the metal-coated side. In contrast, reactive metals like aluminum (Al) oxidize during deposition, forming compressive stress ($\sigma_\mathrm{f} < 0$), leading the tips to bend toward the polymer side.[33–36] The resulting tip-modified geometries are presented in Fig. 2. The actual photographs (Fig. 2a) and SEM images (Fig. 2b and c) compare the overall appearance and surface morphology of Al-TMH and Au-TMH samples and clearly revealing the distinct tip bending induced by metal-specific residual stresses.

Control of tip bending in MH structures

Since tip deformation is governed by the initial geometry of the MH structures, precise control over this geometry is essential. Fig. 3a shows that the taper angle (ψ) of the MH structures can be tuned by adjusting the wettability of the substrate used for the liquid prepolymer. The equilibrium contact angle (θ_e) of the PUA prepolymer increased in the order of PET (primer-treated), Si wafer, glass, and PDMS substrates. ψ also increased accordingly, indicating that it is governed by θ_e and can be controlled by tuning substrate wettability. Although the overall trend is consistent, deviations between θ_e and ψ likely arise from dynamic effects (*e.g.*, the advancing angle) during structure formation. To quantitatively assess the deformation of Al-TMH structures, we define the deflection angle (θ_defl) as the angle between the bent tip and the horizontal line, as this angle reflects the degree of transformation from a re-entrant (MH) to
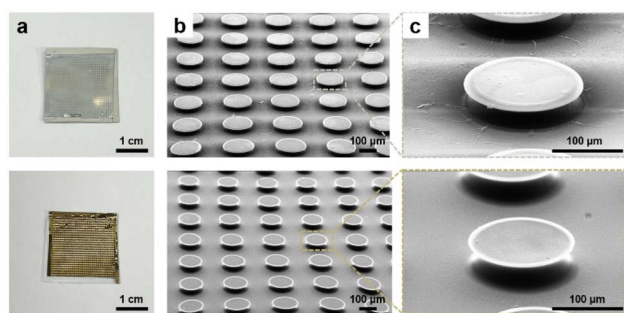

Fig. 2 Photographs and SEM images of Al-TMH (top) and Au-TMH (bottom) samples: (a) photographs, (b) SEM images of the arrays, and (c) magnified views of individual structures.
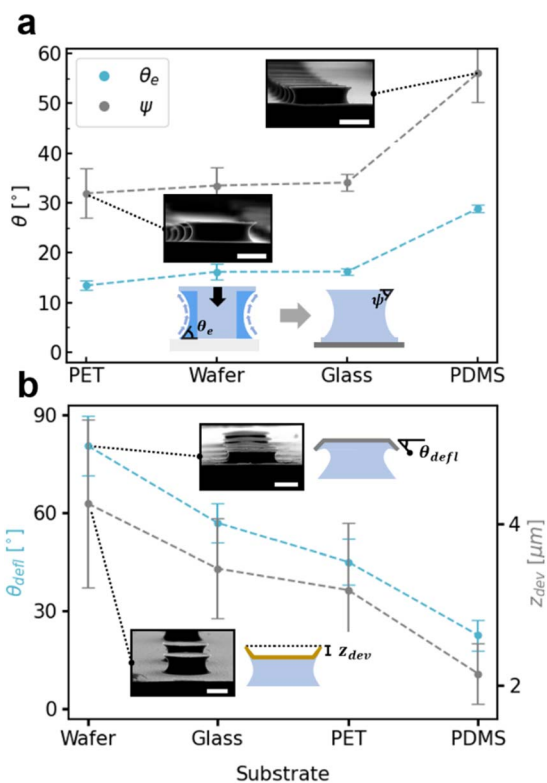
Fig. 3 Tuning the MH structure geometry and its effect on tip deformation: (a) Taper angle ψ of MH structures controlled by adjusting the equilibrium contact angle θ_e through substrate wettability. (b) Influence of taper angle on tip deflection angle θ_{defl} (under Al deposition) and vertical displacement z_{dev} (under Au deposition). All scale bars represent 50 μm.

a doubly re-entrant (Al-TMH) structure. In contrast, for Au-TMH structures, the maximum vertical displacement (z_{dev}) is used as a metric, since their bending occurs predominantly in the vertical direction. As shown in Fig. 3b, smaller ψ values lead to reduced tip deformation, as reflected in both θ_{defl} and z_{dev}. The corresponding cross-sectional SEM images providing a full view of the structural profiles are presented in Fig. S1.

Although fully analytical formulation of the bending behavior of a thin film on a hyperbolic shape is challenging, Stoney's formula, which describes the curvature of a thin film on a planar substrate, provides useful insights into stress-induced bending:[32]

$$\kappa = \frac{6\sigma_f(1 - v_s)d_f}{E_s d_s^2}$$

where κ is the curvature of the film toward the substrate, σ_f is the residual stress, v_s is the Poisson ratio of the substrate, E_s is Young's modulus of the substrate, d_f and d_s are the thicknesses of the film and substrate, respectively. In our case, the underlying MH structure serves as the substrate, with the metal thin film deposited on top. This relation yields two important insights for understanding the bending behavior of TMH structures. First, the sign and magnitude of the residual stress determine the bending direction. Second, for a given deposition condition, increasing the substrate thickness significantly reduces the curvature. This explains why degree of tip deformation (θ_{defl} and z_{dev}) decreases as the taper angle ψ increases: a larger ψ corresponds to a locally thicker structure at the tip. These principles provide a theoretical framework for understanding the tip-localized bending observed in TMH structures.

Replication of TMH structures

As shown in Fig. 4a, TMH structures can be replicated through two consecutive soft molding steps, demonstrating their potential for durable and versatile reproduction in various materials. The replication fidelity is confirmed by SEM images in Fig. 4b, which show that both the inverse mold and the final PUA replica preserve the characteristic tip curvature. Notably, this method enables replication in different polymeric materials while maintaining geometric features, indicating potential applications in surface engineering where precise control of material and structure is required.

Liquid-repellent performance of TMH structures

The Cassie state describes a condition where liquid rests on top of surface textures while air remains in the underlying voids.[37,38]
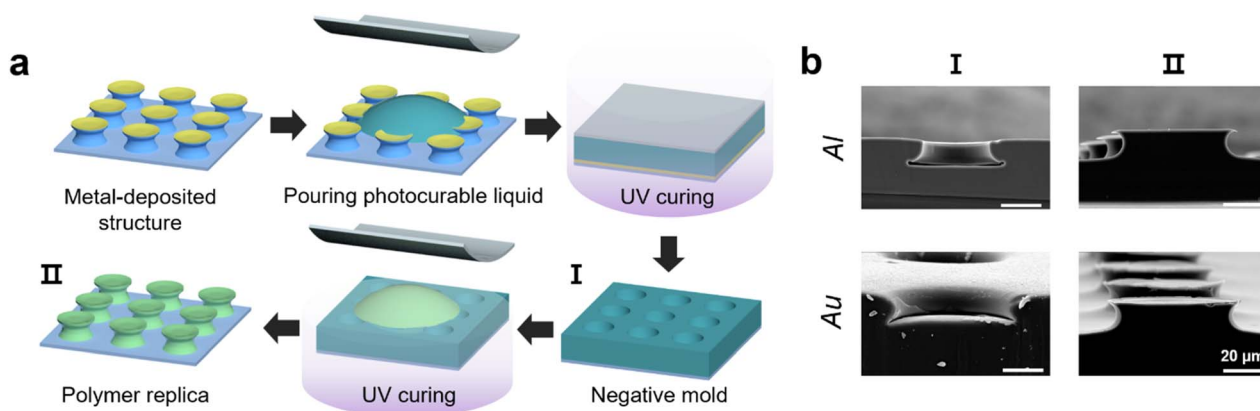

Fig. 4 Replication of TMH structures *via* double soft molding: (a) schematic of the two-step replication process. (b) SEM images of the negative mold (I) and the final polymer replica (II).
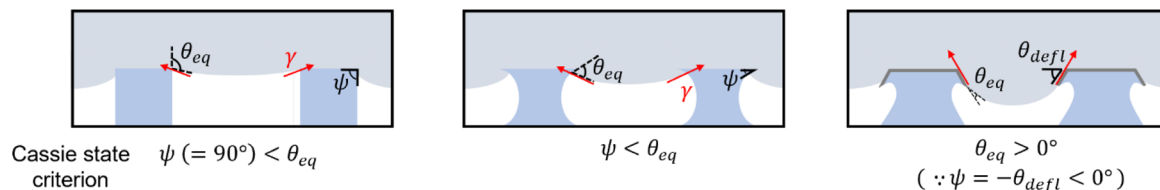
Fig. 5 Schematics of wetting states on normal micropillars, MHs, and TMHs. The Cassie state is sustained for $\theta_{eq} > 90°$ on normal pillars, for ψ on MHs, and for all $\theta_{eq} > 0°$ on doubly re-entrant TMHs.

The transition from the Cassie to the Wenzel state is governed by the geometric criterion between ψ and θ_e, as illustrated in Fig. 5. For normal micropillars ($\psi = 90°$), the Cassie state is sustained only when $\theta_e > 90°$. Re-entrant MH structures with inward-curved openings extend this condition to liquids satisfying $\psi < \theta_e$ by generating an upward Laplace pressure that resists liquid intrusion. In contrast, the doubly re-entrant TMH geometries formed by tip bending can theoretically preserve the Cassie state for all liquids with $\theta_e > 0°$, as their overhanging tips introduce an effective negative taper angle ($\psi = -\theta_{defl} < 0°$)[5,35,39] that generates an upward capillary pressure component stabilizing air entrapment and maintaining a metastable Cassie state.

Based on these geometric principles, we experimentally evaluated the liquid-repellent characteristics of normal pillars, MHs, and TMH structures to verify their predicted influence of tip curvature on wetting behavior. Fig. 6a shows that TMH structures maintain stable repellency against DI water (72.8 mN m^{-1}), olive oil (32 mN m^{-1}), and hexadecane (27.5 mN m^{-1}).[40] In contrast, simple MH structures fail to repel hexadecane, as their taper angle (ψ) exceeds its contact angle on flat PUA (Fig. 6b), resulting in a transition to the Wenzel state. The doubly re-entrant geometry of Al-TMH structures overcomes this limitation and exhibits apparent contact angles (θ^*) of

nearly 150° for all tested liquids, indicating maintenance of the Cassie state. Notably, this performance is preserved in their PUA replicas without the need for fluorinated materials. Furthermore, the repellency remains stable during repeated attachment and detachment of a hexadecane droplet (Fig. 6c), demonstrating its durability.

Conclusions

We have demonstrated a simple and scalable strategy for tip engineering of microstructured surfaces *via* metal-specific thin film deposition. Residual stress generated during thermal evaporation bends the tips of MH structures, enabling their transformation into TMH structures. The direction and extent of bending are governed by both the metal type and the initial geometry of the MH structures, as revealed by experimental tuning and supported by theoretical analysis using Stoney's formula. These TMH structures can be faithfully replicated in various polymeric materials through soft molding, preserving their characteristic tip curvature. The resulting doubly re-entrant architecture, particularly in Al-TMH structures and their PUA replicas, exhibits enhanced and durable liquid repellency—even against low-surface-tension liquids such as hexadecane. This approach provides a versatile platform for surface design with geometrically tunable functionality, offering potential applications in surface functionalization and precise liquid manipulation.

Fig. 6 Enhanced liquid repellency through geometrical and material refinement of MH structures: (a) photographs of DI water (blue), olive oil (orange), and hexadecane (transparent) droplets on Al-TMH structures and their PUA replicas. (b) Apparent contact angles (θ^*) of the three liquids on micropillars, MHs, TMH polymer replicas, and TMHs. (c) Sequential images of hexadecane droplet attachment and detachment on the PUA replicas of TMH structures.

Methods

Fabrication of micropillar structure array

A master mold was fabricated using SU-8 3050 (Kayaku, Microchem) on a silicon wafer *via* photolithography following the manufacturer's guidelines. After post-baking at 150 °C for 1 h, an elastomeric negative mold was created by casting polydimethylsiloxane (PDMS) (Sylgard 184, Dow Corning) prepolymer mixed with a curing agent (10 : 1 weight ratio) over the master mold, followed by baking at 65 °C for 4 h. Polyurethane acrylate (PUA, MINS-301RM, Minuta Tech) precursor, composed of 2-hydroxyethyl methacrylate (HEMA), 1,6-hexanediol diacrylate (HDDA), trimethylolpropane triacrylate (TMPTA), urethane acrylate oligomer, and 2-hydroxy-2-methyl-1-phenyl-1-propanone (Darocur 1173),[41] was poured into the PDMS mold, covered with a PET film (thickness: 50 μm), and exposed to UV light for 90 s to fabricate the micropillar structure array (100 μm in diameter and spacing and 50 μm in height).
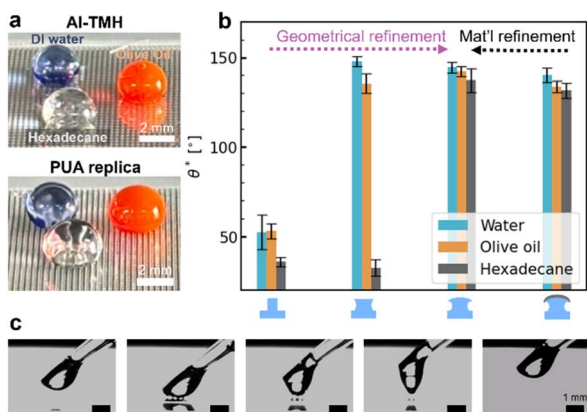
Fabrication of MH and TMH structures

A liquid PUA film was prepared on the substrate *via* spin coating at 2000 rpm for 60 s. Four different substrates (Si wafer, glass, primer-treated PET, and PDMS) were used to modulate the taper angle of the MH structures, taking advantage of the wettability differences of PUA on each substrate. Next, a PUA micropillar structure on a PET film was gently placed in contact with the prepolymer liquid film, allowing the liquid to rise and coat the micropillar sidewalls *via* capillary action. After a few seconds of stabilization, UV light was applied to induce polymerization. Once cured, the film was detached from the substrate, with the hyperbolic structures remaining bonded to the PET film due to the weak adhesion between the crosslinked PUA and the substrate. Metal deposition was performed under high vacuum conditions ($\sim 10^{-6}$ torr) at a constant deposition rate of ~ 5 Å s^{-1}.

Double replication to fabricate polymer replica of TMH structures

All polymer replicas of TMH structures were fabricated from MH structures formed on a silicon wafer substrate. Before the soft molding process, UV light was applied to the bottom of the transparent PET substrate of the TMH structures for 1 h as a post-processing step to enhance adhesion at the metal-polymer interface and promote additional crosslinking. Next, a perfluoropolyether (PFPE)-urethane dimethacrylate (Fluorolink MD 700, Solvay) precursor (mixed with Darocur 1173, 5% w/w) was poured into the TMH structures, which were covered with a PET film (thickness: 50 μm), and exposed to UV light for 20 s to fabricate the negative mold. Subsequently, PUA oligomer was poured into the negative mold, covered with a PET film (thickness: 50 μm), and exposed to UV light for 30 s to fabricate the PUA replica of the TMH structures. Each UV curing step was followed by an additional 2 h UV curing process to ensure further polymerization. The chemical structures of both PUA and PFPE precursors are provided in Fig. S2.

Characterization

Optical microscopy (OM, Olympus BX41M) and scanning electron microscopy (SEM, EM-30, COXEM, Republic of Korea) with an acceleration voltage of 10 kV were employed to obtain the OM and SEM images, respectively. Contact angle images were obtained using a contact angle meter (CAM 200, KSV Instrument Ltd, Finland). The contact angles were measured using ImageJ software.

Author contributions

Chorong Kim: conceptualization, methodology, investigation, visualization. Yoonjin Lee: methodology, investigation, visualization. Jaekyoung Kim: conceptualization, methodology, investigation. Ji Hoon Kim: conceptualization, methodology, investigation, formal analysis, writing – original draft, writing – review & editing, supervision. Hyunsik Yoon: conceptualization, supervision, funding acquisition, writing – original draft, writing – review & editing.

Conflicts of interest

There are no conflicts of interest to declare.

Data availability

The data used to support the findings of this study are included within the article.

Supplementary information is available. See DOI: **https://doi.org/10.1039/d5ra06077j**.

Acknowledgements

Notes and references

1 L. Feng, S. Li, Y. Li, H. Li, L. Zhang, J. Zhai, Y. Song, B. Liu, L. Jiang and D. Zhu, *Adv. Mater.*, 2002, **14**, 1857–1860.

2 H. H. Vu, N.-K. Nguyen, P. Singha, G. Walker, N.-T. Nguyen and N. Kashaninejad, *Adv. Mater. Interfaces*, 2024, **11**, 2400626.

3 M. Li, C. Li, B. R. K. Blackman and S. Eduardo, *Int. Mater. Rev.*, 2022, **67**, 658–681.

4 K. Liu, X. Yao and L. Jiang, *Chem. Soc. Rev.*, 2010, **39**, 3240–3255.

5 A. Tuteja, W. Choi, M. Ma, J. M. Mabry, S. A. Mazzella, G. C. Rutledge, G. H. McKinley and R. E. Cohen, *Science*, 2007, **318**, 1618–1622.

6 K. Autumn, M. Sitti, Y. A. Liang, A. M. Peattie, W. R. Hansen, S. Sponberg, T. W. Kenny, R. Fearing, J. N. Israelachvili and R. J. Full, *Proc. Natl. Acad. Sci. U. S. A.*, 2002, **99**, 12252–12256.

7 N. J. Glassmaker, A. Jagota, C.-Y. Hui and J. Kim, *J. R. Soc. Interface*, 2004, **1**, 23–33.

8 E. Arzt, S. Gorb and R. Spolenak, *Proc. Natl. Acad. Sci. U. S. A.*, 2003, **100**, 10603–10606.

9 S. Reddy, E. Arzt and A. del Campo, *Adv. Mater.*, 2007, **19**, 3833–3837.

10 S. Baik, D. W. Kim, Y. Park, T.-J. Lee, S. Ho Bhang and C. Pang, *Nature*, 2017, **546**, 396–400.

11 P. Vukusic, *Curr. Biol.*, 2006, **16**, R621–R623.

12 S. Kinoshita and S. Yoshioka, *ChemPhysChem*, 2005, **6**, 1442–1459.

13 P. Vukusic and J. R. Sambles, *Nature*, 2003, **424**, 852–855.

14 E. Stratakis, J. Bonse, J. Heitz, J. Siegel, G. D. Tsibidis, E. Skoulas, A. Papadopoulos, A. Mimidis, A.-C. Joel, P. Comanns, J. Krüger, C. Florian, Y. Fuentes-Edfuf, J. Solis and W. Baumgartner, *Mater. Sci. Eng., R.*, 2020, **141**, 100562.

15 J. Zhou, X. Zhao, K. Wang, Y. Chang, D. Xu and G. Wen, *Energy*, 2021, **228**, 120595.

16 C. Chen, D. Liu, L. He, S. Qin, J. Wang, J. M. Razal, N. A. Kotov and W. Lei, *Joule*, 2020, **4**, 247–261.

17 Y. Zhou and L. Jiang, *Joule*, 2020, **4**, 2244–2248.

18 D. Quéré, *Annu. Rev. Mater. Res.*, 2008, **38**, 71–99.

19 G.-T. Yun, W.-B. Jung, M. S. Oh, G. M. Jang, J. Baek, N. I. Kim, S. G. Im and H.-T. Jung, *Sci. Adv.*, 2018, **4**, eaat4978.

20 R. Helbig, J. Nickerl, C. Neinhuis and C. Werner, *PLoS One*, 2011, **6**, e25105.

21 T. Leo Liu and C.-J. CJ Kim, *Science*, 2014, **346**, 1096–1100.

22 K. Liu, Z. Ma, K. Mai, X. Wang, B. Li and J. Chu, *ACS Appl. Mater. Interfaces*, 2024, **16**, 50012–50026.

23 E. M. Domingues, S. Arunachalam and H. Mishra, *ACS Appl. Mater. Interfaces*, 2017, **9**, 21532–21538.

24 S. Dong, X. Zhang, Q. Li, C. Liu, T. Ye, J. Liu, H. Xu, X. Zhang, J. Liu, C. Jiang, L. Xue, S. Yang and X. Xiao, *Small*, 2020, **16**, 2000779.

25 L. Chen, Z. Guo and W. Liu, *J. Mater. Chem. A*, 2017, **5**, 14480–14507.

26 M. Nosonovsky and B. Bhushan, *Philos. Trans. R. Soc., A*, 2016, **374**, 20160185.

27 J. Yong, F. Chen, Q. Yang, J. Huo and X. Hou, *Chem. Soc. Rev.*, 2017, **46**, 4168–4217.

28 J. M. Conder, R. A. Hoke, W. de Wolf, M. H. Russell and R. C. Buck, *Environ. Sci. Technol.*, 2008, **42**, 995–1003.

29 M. Scheringer, X. Trier, I. T. Cousins, P. de Voogt, T. Fletcher, Z. Wang and T. F. Webster, *Chemosphere*, 2014, **114**, 337–339.

30 J. Kim, Y. Ryu, Y. Lee, S. Hwang, K. Lee, D. Ge and H. Yoon, *Chem. Eng. J.*, 2023, **452**, 139270.

31 J. Kim, Y. Ryu, C. H. Kim, S. G. Heo, K.-Y. Yoo and H. Yoon, *Adv. Funct. Mater.*, 2021, **31**, 2010053.

32 M. Ohring, *Materials Science of Thin Films: Depositon and Structure*, Academic Press, 2002.

33 H. Yoon, H. E. Jeong, T. Kim, T. J. Kang, D. Tahk, K. Char and K. Y. Suh, *Nano Today*, 2009, **4**, 385–392.

34 H. Yoon, H. Woo, M. K. Choi, K. Y. Suh and K. Char, *Langmuir*, 2010, **26**, 9198–9201.

35 H. Kim, H. Han, S. Lee, J. Woo, J. Seo and T. Lee, *ACS Appl. Mater. Interfaces*, 2019, **11**, 5484–5491.

36 J. H. Kim, J. G. Bae, H. Yoon and W. B. Lee, *Adv. Mater. Interfaces*, 2024, **11**, 2300942.

37 P.-G. De Gennes, F. Brochard-Wyart and D. Quéré, *Capillarity and Wetting Phenomena, Springer*, New York, NY, 2004.

38 A. Tuteja, W. Choi, M. Ma, J. M. Mabry, S. A. Mazzella, G. C. Rutledge, G. H. McKinley and R. E. Cohen, *Science*, 2007, **318**, 1618–1622.

39 T. Leo Liu and C.-J. CJ Kim, *Science*, 2014, **346**, 1096–1100.

40 *CRC Handbook of Chemistry and Physics*, ed. W. M. Haynes, CRC Press, Boca Raton, 97th edn, 2016.

41 M.-S. Park, K. Kim, Y.-J. Lee, J.-H. Na and S.-U. Kim, *Materials*, 2022, **16**, 35.